Evidence for the Breakdown of Simple Classical Pictures of Organic Molecule-Based Ferrimagnetics: Low-Temperature Crystal Structure and Single-Crystal ESR Studies of an Organic Heterospin System

Masahiro Nishizawa,[†] Daisuke Shiomi,[†] Kazunobu Sato,[‡] Takeji Takui,*[,‡] Koichi Itoh,*[,†] Hiroshi Sawa,[§,⊥] Reizo Kato,*[,§] Hiromi Sakurai,[∥] Akira Izuoka,[∥] and Tadashi Sugawara*[,∥]

Departments of Materials Science and of Chemistry, Graduate School of Science, Osaka City University, Sumiyoshi-ku, Osaka 558-8585, Japan, The Institute for Solid State Physics, The University of Tokyo, Minato-ku, Tokyo 106-8666, Japan, and Department of Pure and Applied Sciences, Graduate School of Arts and Sciences, The University of Tokyo, Meguro-ku, Tokyo 153-8902, Japan

Received: August 23, 1999; In Final Form: October 29, 1999

A model compound for purely organic ferrimagnets has been studied by single-crystal cw-ESR spectroscopy. A heterospin system under study is composed of two kinds of nitronylnitroxide molecules with the ground states of $S = {}^1/_2$ and $S = 1$. These molecules are stacked in an alternating chain in the crystal. The cw-ESR signal of the compound was found to split into two signals below 10 K, which were reproduced by the superposition of two Lorentzian signals. The X-ray measurements at 9.6 K disclosed that the crystal structure remained unchanged at low temperatures, indicating that the origin of the ESR line splitting is not attributable to symmetry reduction associated with structural change but to some change in the spin state: Two distinguishable paramagnetic species are found from the ESR spectra. The appearance of two kinds of paramagnetic species in the alternating chain at finite temperature is expected as a primitive model of thermal excitation in the ferrimagnetic chain which is based on a theoretical calculation. The present experimental results demonstrate that the classical picture of ferrimagnetic spin state (antiparallel alignment of adjacent spins with different spin quantum numbers) is invalidated to describe organic molecule-based exchange-coupled spin systems and overlooks an essential part of the nature of ferrimagnetics.

Introduction

After the discovery of the first genuinely organic ferromagnet *p*-NPNN ($T_C = 0.64$ K),[1] extensive studies have been done in order to construct the organic molecule-based ferromagnets with higher T_C and other molecular functionality magnetics.[2] Together with those ferromagnetic substances based on purely ferromagnetic intermolecular interactions, ferrimagnets have been attracting attention as one of the facile approaches to organic ferromagnets after Buchachenko's proposal for organic ferrimagnetics in 1979.[3] The concept of organic ferrimagnetics is based on the tendency for organic molecules to have antiferromagnetic intermolecular interactions. The antiferromagnetic interactions would bring about antiparallel spin alignment between neighboring molecules with different magnetic moments to result in a possible ordered state with net magnetization (we define this spin arrangement as ferrimagnetic[4]). Magnetic phase transition to ferrimagnetic ordered state, however, has not been documented so far in organic molecular crystalline solids. Only one "model compound" of organic ferrimagnet was synthesized as late as in 1994.[5] The crystal of the model compound for heterospin assemblages consists of alternating chains of two kinds of nitronylnitroxide molecules with the ground states of $S = {}^1/_2$ (**1**) and $S = 1$ (**2**).[5] The molecular structures of **1** and **2** are shown in Figure 1. The ferromagnetic interaction in **2** is about +20 K in the temperature unit,[6] while the intermolecular antiferromagnetic interaction is in the order of −10 K.[5] The crystal structure of the molecular complex (**1**+**2**) seemingly favors the ferrimagnetic spin alignment.[5] The χT value, however, has been found to decrease below 3 K for (**1**+**2**), demonstrating that antiparallel alignment of $S = {}^1/_2$ and $S = 1$ spins has not been achieved in the crystal.[5]

In a previous paper,[7] we discussed a possibility of ferrimagnetic order occurring in organic molecular solids from an exact diagonalization of a Heisenberg−Dirac spin Hamiltonian for an $S = {}^1/_2$ and $S = 1$ alternating chain. In the chain, the intramolecular magnetic degree of freedom remains within the $S = 1$ site. The $S = 1$ spin is composed of two $S = {}^1/_2$ spins coupled by finite ferromagnetic interaction: The unit cell of the chain consists of three $S = {}^1/_2$ spins. The main issue of the calculation was a quasi-degeneracy of the ground and the low-lying eigenstates of the Hamiltonian which was found for the chain with nine $S = {}^1/_2$ spins in three unit cells.[7] We interpreted the quasi-degeneracy as three noninteracting $S = {}^1/_2$ spins appearing in the finite-size lattice at the zero-temperature limit.[7] The appearance of the paramagnetic $S = {}^1/_2$ spin is explained by assuming that two of the three spins in the unit cell are quenched owing to the formation of a singlet ($S = 0$) pair so that they no longer contribute to the bulk magnetization. The formation of the singlet pair would leave a decoupled $S = {}^1/_2$ spin. The singlet pair formation is a quantum effect of electron

* Corresponding author. E-mail address: takui@sci.osaka-cu.ac.jp. Phone: +81-6-6605-2605. FAX: +81-6-6605-3137.
[†] Department of Materials Science.
[‡] Department of Chemistry.
[§] The Institute for Solid State Physics.
[∥] Department of Pure and Applied Sciences.
[⊥] Present address: Department of Physics, Faculty of Science, Chiba University, Inage-ku, Chiba 263-8522, Japan.

10.1021/jp992980j CCC: $19.00
Published on Web 12/22/1999

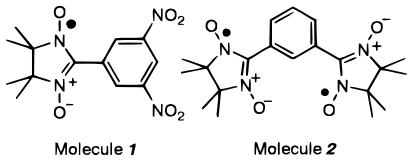

Figure 1. Molecules **1** and **2**.

spins coupled by antiferromagnetic exchange interactions and would compete against long-range ferrimagnetic spin−spin correlation.

The system size of only three unit cells with nine $S = {}^1/_2$ spins are too small to give a reliable solution to absence or existence of the long-range spin−spin correlation in the exchange-coupled many-body systems.[8] Therefore, we have to regard the apparently decoupled spins described above as a crude picture for the ground state of molecule-based ferrimagnetic chains. At finite temperatures, the antiferromagnetically coupled spins should recover their contribution to the bulk magnetization by breaking the singlet pairs. Such thermally activated paramagnetic spins are to be regarded as a one-dimensional array of $S = {}^1/_2$ spins since the thermal energy partially destroys the intermolecular singlet pairs along the chain. Thus, to the first approximation, two kinds of paramagnetic species are expected to appear at finite temperatures in the crystal: One is apparently free of magnetic coupling and the other undergoes one-dimensional antiferromagnetic interactions. The main purpose of the present study is to give an experimental evidence for the coexistence of the two kinds of paramagnetic spins in the crystal of (**1**+**2**) at finite temperatures. The crude picture of the ground state is tested by examining the thermally excited states as might be expected from the ground state.

We examine single-crystal cw (continuous-wave) ESR and low-temperature crystal structure of the model compound (**1**+**2**) in order to clarify the spin state of the molecular chain. The discrepancy between the spin state obtained in the present study and the simple classical picture of the ferrimagnetic spin alignment, antiparallel alignment of different spin moments, is emphasized.

Experimental Section

The single-crystal cw-ESR spectra were recorded in the X-band on a BRUKER ESR spectrometer ESP 300 equipped with a TM mode cavity. The cryogenic temperature was controlled by an OXFORD helium-gas-flow variable temperature controller ESP 910.

The crystal structure determination at low temperatures was performed using a MAC Science Weissenberg-type imaging plate system equipped with a DAIKIN closed-cycle helium-flow refrigerator.

Results and Discussion

1. ESR at Room Temperature. *(1) g-Tensor.* The cw-ESR spectrum exhibited a single Lorentzian line at room temperature (298 K). The angular variation of the *g*-value is depicted in Figure 2. The principal values of the **g**-tensor, g_1, g_2, and g_3 (defined as $g_1 > g_2 > g_3$), and their direction cosines are listed in Tables 1 and 2, respectively. When two or more $S = {}^1/_2$ spins are exchange-coupled, the **g**-tensor of the resultant spin is, to the first approximation, given by the average of the component tensors.[9] We examined the averaging effect of **g**-tensor due to the exchange interactions in the (**1**+**2**) heterospin assemblage. The **g**-tensor of *p*-NPNN,[10] $\mathbf{g}_{p-\mathrm{NPNN}}$, is adopted as component tensors of the three nitronylnitroxide groups (ONCNO) in the unit cell with the smallest principal value (g_3) normal to the ONCNO plane and the other two (g_1, g_2) within the plane. The averaged **g**-tensor of the repeating unit, $\mathbf{g}^{\mathrm{av}}$, is calculated as

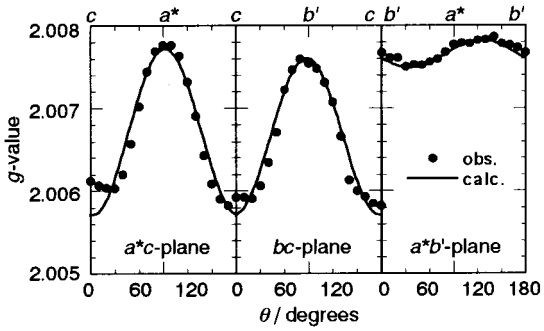

Figure 2. The angular dependence of the *g*-value of the (**1**+**2**) heterospin assemblage at room temperature. The closed circles denote the observed data. The solid lines represent the theoretical curves calculated by averaging the component **g**-tensors from the three nitronylnitroxide groups in the unit cell. The *b*′-axis is perpendicular to the *c*-axis in the *bc*-plane. θ is the angle between the magnetic field and the *c*-axis or *b*′-axis.

TABLE 1: Principal Values of the g-Tensors for the (1 + 2) Heterospin System

		g_1	g_2	g_3
298 K	observed	2.0088	2.0083	2.0060
	calculated g^{av}	2.0088	2.0083	2.0060
	calculated g^{α}	2.0110	2.0068	2.0017
	calculated g^{β}	2.0102	2.0062	2.0045
	calculated g^{γ}	2.0105	2.0048	2.0045
5 K	observed A	2.0149	2.0077	2.0031
	observed B	2.0124	2.0063	2.0046
3 K	observed A	2.0173	2.0055	2.0027
	observed B	2.0137	2.0076	2.0041
p-NPNN[10]		2.0117	2.0051	2.0038

TABLE 2: Direction Cosines of the g-Tensors in the *ab′c* Frame[a] for the (1+2) Heterospin System**

			*a**	*b*′	*c*
298 K	observed	g_1	−0.242	−0.969	−0.0448
		g_2	−0.968	0.244	−0.0549
		g_3	−0.0641	−0.0301	−0.997
	calculated	g_1^{av}	−0.242	−0.969	−0.0448
		g_2^{av}	−0.968	0.244	−0.0549
		g_3^{av}	−0.0641	−0.0301	0.997
	calculated	g_1^{α}	0.881	−0.253	0.400
		g_2^{α}	0.291	0.956	−0.0352
		g_3^{α}	−0.374	0.147	0.916
	calculated	g_1^{β}	0.715	0.506	−0.482
		g_2^{β}	−0.618	0.780	−0.0987
		g_3^{β}	0.326	0.369	0.870
	calculated	g_1^{γ}	−0.998	0.0684	−0.0171
		g_2^{γ}	−0.0523	−0.880	−0.472
		g_3^{γ}	−0.0473	−0.470	0.882
5 K	observed A	g_1	0.772	0.622	−0.128
		g_2	0.613	−0.677	0.407
		g_3	−0.167	0.393	0.904
	observed B	g_1	−0.250	−0.190	0.950
		g_2	0.911	0.288	0.297
		g_3	−0.329	0.939	0.101
3 K	observed A	g_1	0.747	0.661	−0.0683
		g_2	0.624	−0.663	0.413
		g_3	−0.227	0.351	0.908
	observed B	g_1	−0.274	−0.154	0.949
		g_2	0.954	0.0796	0.289
		g_3	−0.120	0.985	0.125

[a] The *b*′-axis is perpendicular to the *c*-axis in the *bc*-plane.

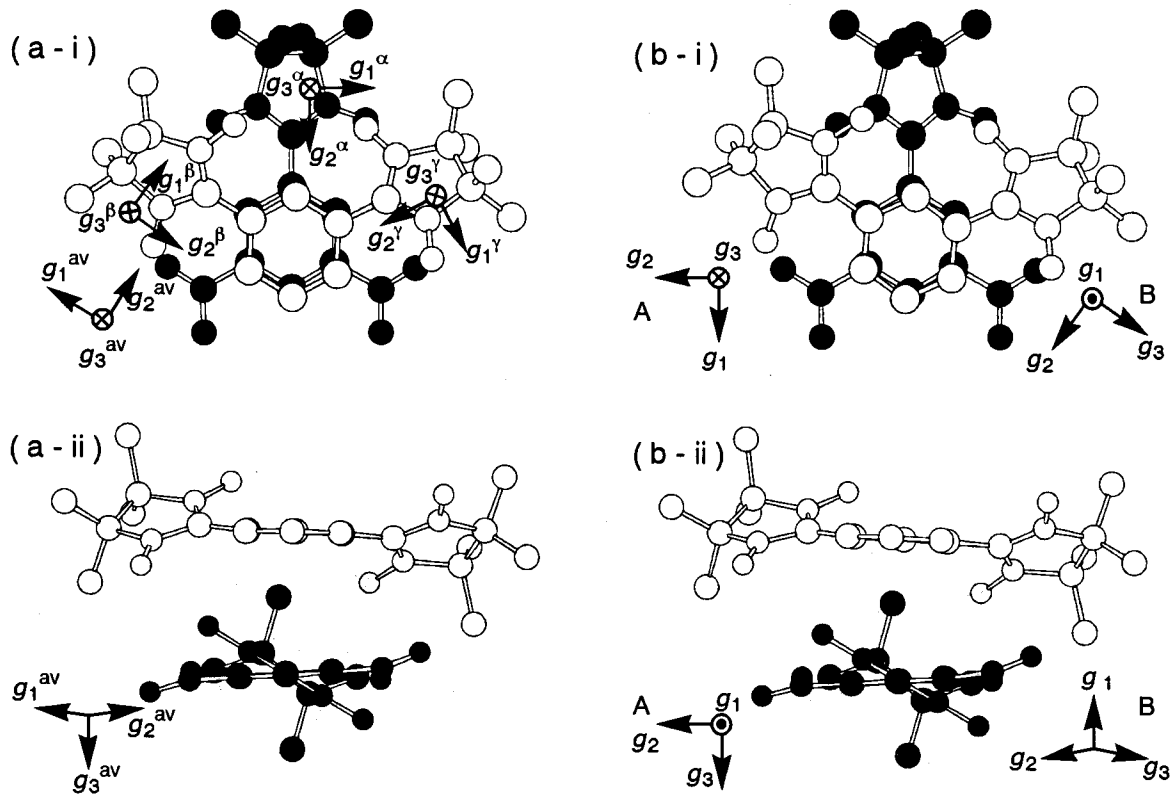

Figure 3. The molecular stacking of the molecule **1** (closed circles) and **2** (open circles) at (a) 298 K[5] and (b) 9.6 K. (i) Projected along the *c*-axis. (ii) Viewed along the molecular plane. The arrows indicate the principal directions of the three component tensors, $\mathbf{g}^{\alpha}$, $\mathbf{g}^{\beta}$, and $\mathbf{g}^{\gamma}$, of the nitronylnitroxide radical groups and those of the exchange-averaged tensor $\mathbf{g}^{\mathrm{av}}$.

$$\mathbf{g}^{\mathrm{av}} = \frac{1}{3}(\mathbf{U}_{\alpha}^{-1}\mathbf{g}^{\alpha}\mathbf{U}_{\alpha} + \mathbf{U}_{\beta}^{-1}\mathbf{g}^{\beta}\mathbf{U}_{\beta} + \mathbf{U}_{\gamma}^{-1}\mathbf{g}^{\gamma}\mathbf{U}_{\gamma}) \qquad (1)$$

$$\mathbf{g}^{\alpha} \approx \mathbf{g}^{\beta} \approx \mathbf{g}^{\gamma} \approx \mathbf{g}_{p-\mathrm{NPNN}} \qquad (2)$$

where $\mathbf{g}^{\alpha}$ is the **g**-tensor of the nitronylnitroxide group in the molecule **1**, while $\mathbf{g}^{\beta}$ and $\mathbf{g}^{\gamma}$ are those of the two nitronylnitroxide groups in the molecule **2**. The unitary matrixes $\mathbf{U}_{\alpha}$, $\mathbf{U}_{\beta}$, and $\mathbf{U}_{\gamma}$ define the directions of the principal axes of the three tensors with respect to those of the averaged tensor $\mathbf{g}^{\mathrm{av}}$. The calculated **g**-tensor $\mathbf{g}^{\mathrm{av}}$ reproduces the observed angular variation of *g*-value as shown by the solid lines in Figure 2. The principal directions of the tensors, $\mathbf{g}^{\mathrm{av}}$, $\mathbf{g}^{\alpha}$, $\mathbf{g}^{\beta}$, and $\mathbf{g}^{\gamma}$, are drawn by the arrows in Figure 3a. As summarized in Table 1, g_1 is equal to g_2 both for the observed and the calculated tensors. Since the three ONCNO planes are approximately coplanar as shown in Figure 3a, g_1 and g_2 are remarkably averaged to give $g_1^{\mathrm{av}} \approx g_2^{\mathrm{av}}$. The thermal energy of room temperature is sufficiently large compared with the intra- ($\approx$+20K) and intermolecular (≈-10K) exchange interactions, and the effect of the singlet pair formation is negligible. Thus, the spin system of (**1**+**2**) at room temperature is described by the exchange-averaged spin system, in which all the three paramagnetic spins in the unit cell participate.

(2) Line Width. The angular dependence of the ESR peak-to-peak line width ΔB_{pp} showed a maximum in the magnetic field direction parallel to the molecular stacking axis (// *c*-axis) and minima around the two magic angles (54.7° and 125.3°) in the *a***c*- and *bc*-plane as shown in Figure 4. Generally, minima of ESR line width at the magic angles suggest that the spin system is low dimensional.[11] On the other hand, for the 3-D magnetic structure, i.e., the spin system without preferential direction of the magnetic interaction, the line width is proportional to $(1+\cos^2\theta)^2$, where θ denotes the orientation of the applied field defined with respect to one of the principal axes of magnetic interactions.[11] The correlation between the magnetic dimensionality and the angular variation of ESR line width have been derived and discussed so far for the spin array with each spin localized at a single (one-centered) atomic site. In the organic molecule-based magnetics, however, an unpaired electron spin is spread over several (multicentered) atomic sites within a radical molecule (e.g., O, N, N, and O atoms for nitronylnitroxide derivatives). Furthermore, the molecular chain in the (**1**+**2**) heterospin assemblage is not a simple chain but a collinear one with a two-spin site at every other molecule along the chain. Before specifying the magnetic dimensionality of the (**1**+**2**) assemblage in terms of the angular dependence of ΔB_{pp}, we calculate the angular dependence of dipolar second moment[12] ΔM as an estimate of the dipolar-broadened ESR line width by taking the crystal structure into account. The dipolar second moment ΔM_k in the magnetic field unit, or $\langle\Delta\omega^2\rangle$ in the frequency unit, is given by

$$\Delta M_k = \frac{\hbar}{g\mu_{\mathrm{B}}}\sqrt{\langle\Delta\omega^2\rangle} \qquad (3)$$

$$\langle\Delta\omega^2\rangle = \frac{1}{\hbar^2}\sum_j \frac{\mu_j^2\,\mu_k^2}{\mathrm{r}_{jk}^6}(3\cos^2\phi_{jk} - 1)^2 \qquad (4)$$

where the summation j runs over all pairs of the magnetic dipoles, μ_j and μ_k, within the sphere of the diameter of 400 Å in the crystal, putting the kth dipole at the center of the sphere. r_{jk} and ϕ_{jk} stand for the distance between the jth and kth dipoles and the angle between the static field and the vector r_{jk}, respectively. For simplifying the calculation, magnetic dipoles of $\mu_j = \mu_k = \mu_{\mathrm{B}}/4$ are distributed to four atomic sites, O, N, N, and O, of the nitronylnitroxide group as depicted in the inset

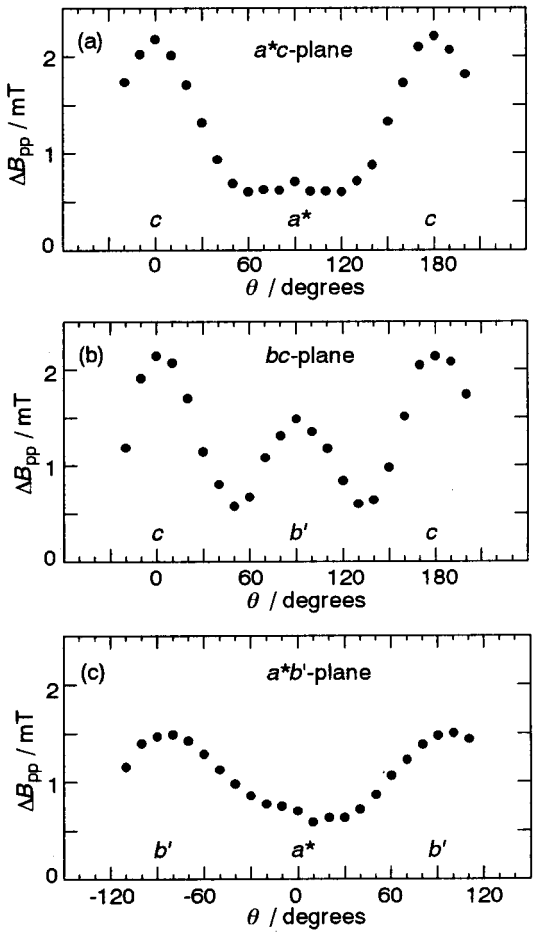

Figure 4. The angular dependence of the ESR line width ΔB_{pp} of the (**1**+**2**) heterospin assemblage at room temperature in the (a) a^*c-plane, the (b) bc-plane, and the (c) a^*b'-plane. The b'-axis is perpendicular to the c-axis in the bc-plane. θ is the angle between the magnetic field and the (a, b) c-axis or (c) a^*-axis.

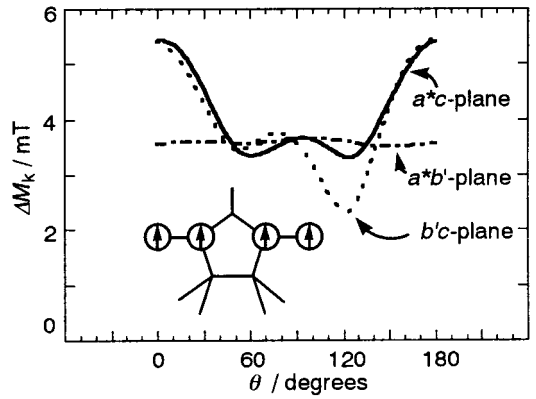

Figure 5. The angular dependence of the dipolar second moment ΔM_k calculated using the crystal structure at room temperature. The b'-axis is perpendicular to the c-axis in the bc-plane. θ is the angle between the magnetic field and the c-axis (the a^*c- and $b'c$-planes) or a^*-axis (the a^*b'-plane). The inset shows the distribution of a dipole moment in the nitronylnitroxide group which is assumed in the calculation. The arrow indicates the magnetic dipole of $\mu_B/4$.

of Figure 5. As shown in Figure 5, the angular dependence of ΔM_k calculated on the basis of the crystal structure exhibits a maximum at the field direction parallel to the c-axis ($\theta = 0°$) and minima at the two magic angles ($\theta = 54.7°$ and $125.3°$). From the second-moment calculations, it has been shown that the angular dependence of the dipolar contribution to the ESR line width retains characteristic of one-dimensional spin system

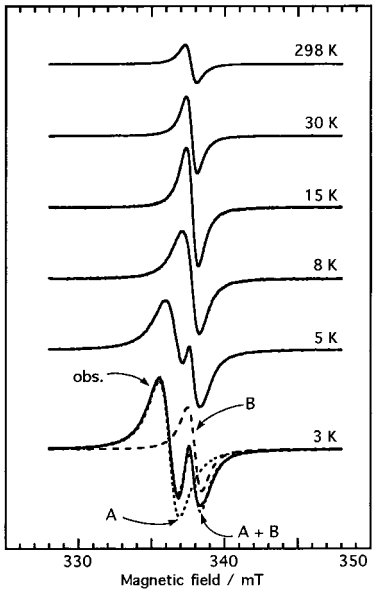

Figure 6. The temperature dependence of the ESR spectra of the (**1**+**2**) heterospin assemblage. The direction of the applied field is 50° from the a^*-axis in the a^*b'-plane. The dashed lines, A, B, and A+B, denote the deconvolution calculated by assuming two-component Lorentzian line shapes.

even if the spin dipole moments are spread over several atomic sites, O−N−(C)−N−O, in the nitronylnitroxide groups. Although for the quantitative agreement of the calculated line widths with the observed ones, we need to consider explicitly the contribution of the intermolecular exchange interactions with the spin density spread over the several atomic sites, the result from dipolar second moment calculations shows that the molecular array of the (**1**+**2**) heterospin assemblage is regarded as a one-dimensional collinear chain of magnetically coupled spins.

2. ESR and Crystal Structure at Low Temperatures. *(1) ESR Signal Splitting and Low-Temperature X-ray Experiments.* The cw-ESR spectrum, which exhibited symmetric Lorentzian line at room temperature, distorted its line shape around 10 K and split into two lines below 8 K as depicted in Figure 6. The splitting pattern was reversible on cooling and warming and reproducible using several pieces of single crystals. The single-crystal X-ray diffraction pattern as well as diffraction line width remained unchanged before and after the low-temperature ESR experiments. These results eliminate cracking of the crystals as an origin of the splitting. Furthermore, the signal intensity excluded the possibility that the splitting originated in some extrinsic paramagnetic center such as lattice defects. From these findings, the splitting is attributed to some inherent temperature-dependent properties of the (**1**+**2**) heterospin system, which are structural or magnetic.

Two mechanisms are proposed for the splitting of ESR spectrum on lowering the temperature: [I] A "site-splitting" due to symmetry reduction associated with structural change and [II] a spin-state change due to magnetic interaction. To specify the mechanism, the X-ray diffraction of the single crystal of the (**1**+**2**) complex was measured at 298, 30, and 9.6 K (the lowest temperature for our apparatus). The crystal structure, including the molecular conformations of **1** and **2**, was found to remain unchanged on lowering the temperature as shown in Figure 3b. The lattice parameters of the (**1**+**2**) complex are listed in Table 3. Only shrinkage of the unit cell was observed at low temperatures: The unit cell decreased in volume by 4% from 298 K down to 9.6 K. The shrinkage was almost isotropic

TABLE 3: Lattice Parameters of the (1+2) Molecular Complex at Low Temperatures and Room Temperature

	298.0 K[5]	30.0 K	9.6 K
a, Å	11.526(3)	11.15(1)	11.15(1)
b, Å	13.260(2)	12.82(1)	12.82(1)
c, Å	7.288(2)	7.134(7)	7.133(7)
α, degrees	106.57(2)	105.9(1)	105.9(1)
β, degrees	106.34(3)	101.9(1)	101.8(1)
γ, degrees	90.38(2)	70.09(7)	70.08(7)
V, Å^3	1020.0(5)	976.1(9)	976.0(9)
R	0.059	0.034	0.034
space group	*P*1	*P*1	*P*1

along the *a*-, *b*-, and *c*-axes. The orientation of the molecule **1** relative to **2** along the chain remained basically unchanged within experimental error as shown in Figure 3. From the result of the low-temperature X-ray measurements, the possibility of [I] for the ESR line splitting is eliminated. The splitting below 10 K is attributed to some change inherent in the spin state of the system under study.

The split spectrum was well reproduced by the superposition of two Lorentzian lines A (strong) and B (weak). Figure 6 shows an example of the deconvolution assuming the two-component Lorentzian line shape for the spectrum measured at 3 K. The *g*-values, line widths, and signal intensity were obtained for each of the components, A and B, as line shape parameters of the Lorentzian functions. These line shape parameters are discussed below in order to deduce the low-temperature spin state.

*(2) **g**-Tensor.* The angular variation of the *g*-values of the signals A and B at 3 K is drawn in Figure 7. The principal values of the **g**-tensors and their direction cosines are listed in Table 1 and Table 2, respectively. For the field orientation where the transition fields, i.e., the *g*-values, of A and B are close to each other, the deconvolution was unsuccessful. Particularly for the weak signal B, the uncertainty of the *g*-value is rather large in such field orientation. One can state, however, that the principal values and axes of the **g**-tensors for A and B are quite different from each other at low temperature, indicating that the spin state of the paramagnetic species responsible for the signal A is quite different from that of B.

As shown above, the **g**-tensor at room temperature was well reproduced by averaging the component tensors from the three nitronylnitroxide radical groups in the unit cell by assuming the exchange interactions between the three radical centers. The coplanarity of the three ONCNO groups in the repeating unit afforded $g_1^{av} \approx g_2^{av}$. Although the crystal structure, i.e., the relative orientation of the three ONCNO planes, is unchanged, the **g**-tensors of the low-temperature signals are different from those at room temperature; the **g**-tensor anisotropy is enhanced. Furthermore, the principal axes of A are far apart from those of B. The principal axes of A and B are not collinear to any of the ONCNO plane nor the average of any two of the three planes as shown by the arrows in Figure 3b: Simple magneto-structural correlation in terms of the **g**-tensors is no longer found. Considering the straightforward description of the exchange-averaged **g**-tensor at room temperature, which is nearly isotropic in the *ab*-plane or g_1-g_2 plane, the low-temperature **g**-tensors suggest some spatial rearrangement of the exchange-averaging effect, leading to the ESR line splitting. In other words, the intermolecular exchange interaction responsible for the **g**-tensor anisotropy is less spanned over the molecular chain at low temperatures.

(3) Line Width. The angular dependence of the peak-to-peak line widths ΔB_{pp} for the (**1**+**2**) system at 3 K is shown in Figure 8. The angular dependence of the line width at 5 K close resembled that at 3 K. The ΔB_{pp} for A is proportional to $\sin^2\theta$ (θ is the angle between the applied magnetic field and the *c*-axis or *a**-axis) in all the planes, *a***c*-, *bc*-, and *a***b*′-planes, which suggests that for the paramagnetic species responsible for the signal A there is no preferential direction of the magnetic interaction such as one-dimensional chain. On the other hand, the ΔB_{pp} for B shows a maximum in the magnetic field direction parallel to the molecular stacking chain (// *c*-axis) and minima around the two magic angles from the *c*-axis in the *a***c*-plane, although the minimum in ΔB_{pp} at the magic angle is not clearly observed in the *bc*-plane owing to the poor resolution of the deconvolution. From the finding, we conclude that one of the two kinds of the paramagnetic species retains the low-dimensional magnetic interaction and the other has no preferential direction of the magnetic interactions.

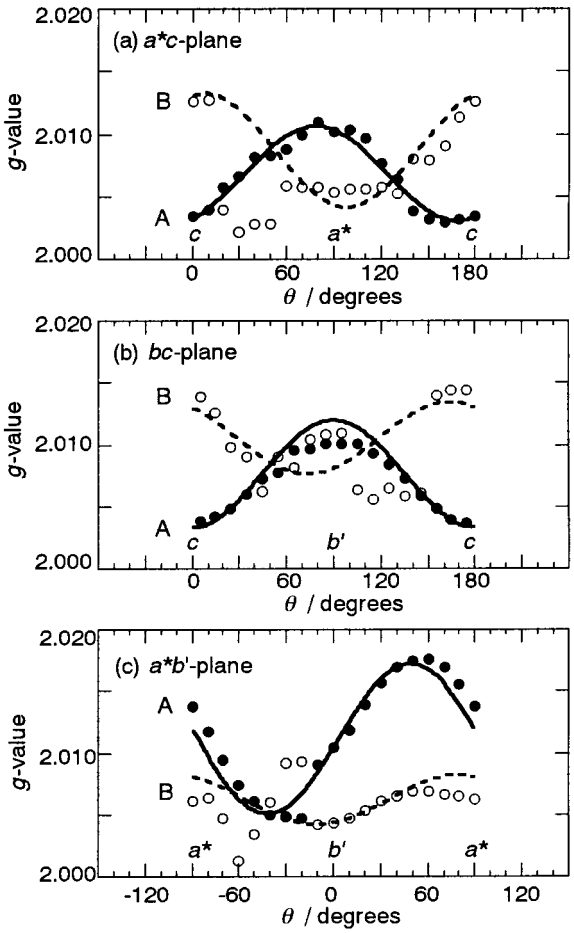

Figure 7. The angular dependence of *g*-value for the deconvoluted signals A and B in the (a) *a***c*-plane, (b) *bc*-plane, and (c) *a***b**-plane at 3 K. The *b*′-axis is perpendicular to the *c*-axis in the *bc*-plane. θ is the angle between the magnetic field and the (a, b) *c*-axis or (c) *b*′-axis. The solid (A) and dashed (B) lines are calculated from the optimized **g**-tensors. The closed (A) and open (B) circles are observed values. The weak signal B was not successfully deconvoluted, when the *g*-values of A and B are close to each other.

(4) Intensity. The signal intensity of A was enhanced with decreasing temperature, almost obeying the Curie Law ($\propto 1/T$). The relative intensity of the signal B to the signal A decreased on lowering the temperature (1/6 at 5 K to 1/10 at 3 K). The temperature dependence of the relative intensity shows that paramagnetic species giving rise to the signal B undergoes antiferromagnetic interaction. From this result, together with the angular variation of the line widths, the signal A is assigned to the apparently free $S = {}^1/_2$ spin as expected from the calculation,[7] while the signal B corresponds to the thermally

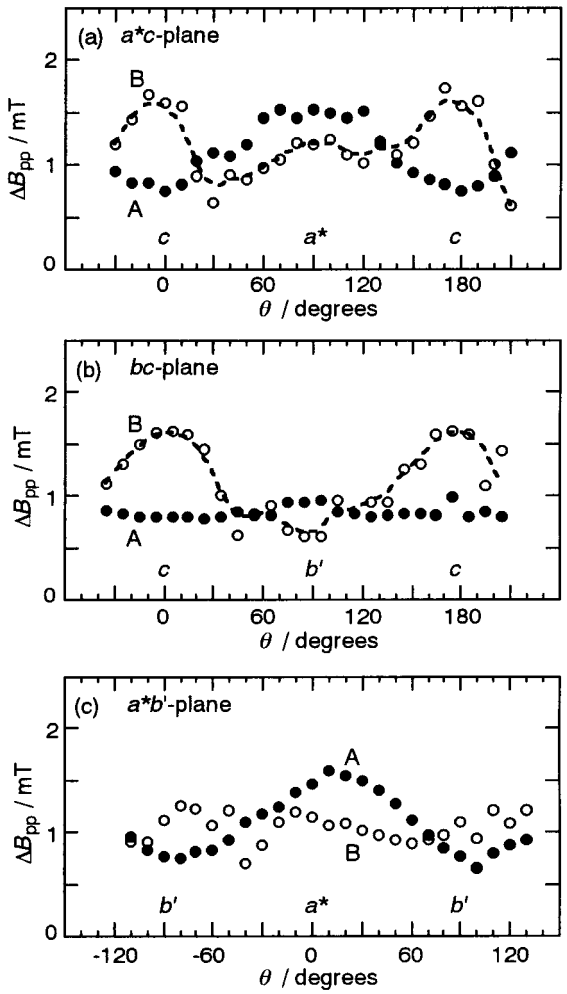

Figure 8. The angular dependence of line width for A and B in the (a) a^*c-plane, (b) bc-plane, and (c) a^*b'-plane at 3 K. The b'-axis is perpendicular to the c-axis in the bc-plane. θ is the angle between the magnetic field and the (a, b) c-axis or (c) a^*-axis. The closed (A) and open (B) circles denote the Lorentzian lines obtained from the deconvolution of the observed spectra. The dashed lines are to guide the reader's eye.

activated spins coupled by the one-dimensional antiferromagnetic interactions along the chain.

3. Low-Temperature Spin State. As described above, we detected in the single-crystal cw-ESR experiments the two kinds of paramagnetic species at low temperatures. One has no preferential direction of magnetic interaction. The other is the thermally activated spins in a one-dimensional antiferromagnetic chain. The appearance of the two kinds of species are expected as a primitive model of thermal excitation for the ferrimagnetic chain which is based on the crude picture of the ground state.[7] The present single-crystal ESR study gives an experimental evidence for the appearance of the two kinds of species in the real organic heterospin assemblage.

A schematic picture of the ground state of the alternating chain composed of the $S = {}^1/_2$ and $S = 1$ molecules is drawn in Figure 9a, which is based on the theoretical calculation[7] and the present experimental results. The calculation has suggested that the singlet pairs are formed between the molecule **1** and **2** as indicated by the ovals in Figure 9a, when the spatial symmetry of the 2-fold intermolecular interactions is lowered.[7] The singlet pairs are preferentially formed at the spin sites with the larger intermolecular interactions as depicted on the lower side of the chain. When the alternation of the intermolecular

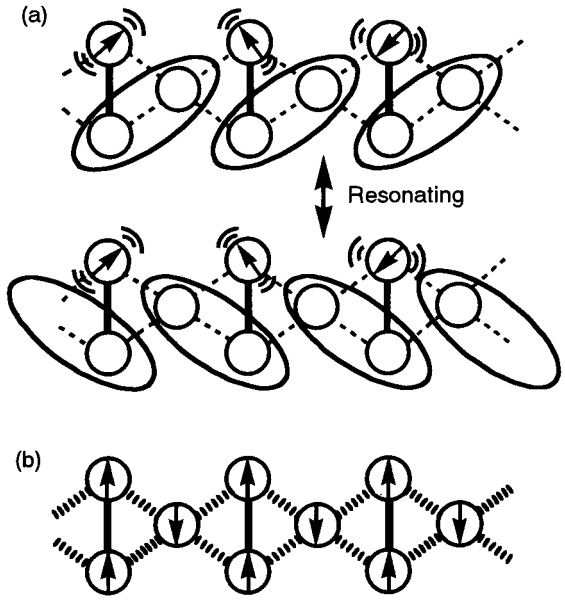

Figure 9. (a) Schematic representation of the ground state of the $S = {}^1/_2$ and $S = 1$ alternating chain. The open circles are spin-$^1/_2$ sites. The solid lines represent the intramolecular ferromagnetic interactions. The dashed lines show the intermolecular antiferromagnetic interactions. The ovals show the intermolecular singlet ($S = 0$) spin-pairs. (b) Classical picture of the ferrimagnetic spin alignment.

antiferromagnetic interactions in strength along the chain is neglected, the singlet pairs resonate along the chain. The resonance should leave an $S = {}^1/_2$ spin apparently decoupled. This "apparently decoupled" spin brings about a single $S = {}^1/_2$ spin without preferential direction of spin−spin interactions. The resonating singlet pairs are thermally destroyed at finite temperatures to give a one-dimensional antiferromagnetically coupled $S = {}^1/_2$ spin array.

A salient feature of organic open-shell molecules is isotropic nature of intermolecular exchange interactions.[7,13] The feature results from low symmetry of the organic molecules and weak spin−orbit interactions compared with those of transition metal ions. From this feature, the antiferromagnetically coupled isotropic spins inherently favors the singlet-pair formation rather than the Neel state or the antiparallel alignment of the adjacent spins. Furthermore, the intra- and intermolecular magnetic interactions in the (**1**+**2**) heterospin assemblage are comparable in strength.[5,6] Because of all these characteristics, the $S = 1$ spin is not a good quantum number for the two-spin site (molecule **2**) in the chain. Thus, the simple, classical ferrimagnetic spin state as given in Figure 9b is not the most stable case for the collinear spin chain of the (**1**+**2**) assemblage.

Conclusion

In the single-crystal cw-ESR spectra from the model compound for a purely organic molecule-based ferrimagnet, the (**1**+**2**) heterospin assemblage, the splitting of the ESR signal was observed at low temperatures. The single-crystal X-ray measurements showed that the crystal structure remained unchanged at low temperatures and the origin of the ESR line splitting was attributable to the change in the spin state in the crystal: Two distinguishable paramagnetic species appeared on lowering the temperature. The analyses of the **g**-tensors and line widths of the two kinds of ESR signals disclosed that the two paramagnetic species correspond to those expected as a primitive model of thermal excitation of the ferrimagnetic chain. To obtain more sophisticated pictures for the ground and low-lying excited

states of the ferrimagnetic chain, we need to separate more precisely the contribution of the two species to the bulk susceptibility by ESR experiments in ultralow-temperature regions.

The drawback to achieving a ferrimagnetic spin alignment in molecule-based solids are the insufficient stability of $S = 1$ state (i.e., nonrobust spin polarization in the $S = 1$ molecule), the isotropic exchange interaction, and the multicentered intermolecular magnetic interactions[7] leading to the singlet pairs between one of the two $S = {}^1/_2$ spins of $S = 1$ molecule and a spin of $S = {}^1/_2$ molecule. The resultant peculiar spin state has been observed in the real heterospin assemblage, (**1**+**2**).

Acknowledgment. This work has been supported by Grants-in-Aid for Scientific Research on Priority Area "Molecular Magnetism" (Areas 228/04 242 103, 04 242 104, and 04 242 105) from the Ministry of Education, Science, Sports and Culture, Japan and also by NEDO Project "Organic Magnets" from the Ministry of International Trade and Industries, Japan. The authors (D.S. and K.S.) acknowledge the Ministry of Education, Science, Sports and Culture, Japan for Grants-in-Aid for Encouragement of Young Scientists (Grants 07740468, 07740553, 08740462, 09740528, and 10740275).

References and Notes

(1) (a) Tamura, M.; Nakazawa, Y.; Shiomi, D.; Nozawa, K.; Hosokoshi, Y.; Ishikawa, M.; Takahashi, M.; Kinoshita, M. *Chem. Phys. Lett.* **1991**, *186*, 401. (b) Nakazawa, Y.; Tamura, M.; Shirakawa, N.; Shiomi, D.; Takahashi, M.; Kinoshita M.; Ishikawa, M. *Phys. Rev. B*, **1992**, *46*, 8906.

(2) (a) Gatteschi, D., Kahn, O., Miller, J. S., Palacio, F., Eds. *Molecular Magnetic Materials*; Kluwer Academic: Dordrecht, 1991. (b) Iwamura, H.; Miller, J. S., Eds. *Mol. Cryst. Liq. Cryst*. **1993**, *232, 233*. (c) Miller, J. S.; Epstein, A. J., Eds. *Mol. Cryst. Liq. Cryst*. **1995**, *271*−*274*. (d) Itoh, K.; Miller, J. S., Takui, T., Eds. *Mol. Cryst. Liq. Cryst*. **1997**, *305*, *306*. (e) Kahn, O., Ed. *Mol. Cryst. Liq. Cryst.* **1999**, *334*, *335*.

(3) Buchachenko, A. L. *Dokl. Akad. Nauk. Engl. Ed.* **1979**, *244*, 107.

(4) By "ferrimagnetic", we mean that the intermolecular interaction is primarily antiferromagnetic but net magnetization arises from the differing moments ordered in the sublattices.

(5) Izuoka, A.; Fukada, M.; Kumai, R.; Itakura, M.; Hikami, S.; Sugawara, T. *J. Am. Chem. Soc*. **1994**, *116*, 2609.

(6) Izuoka, A.; Fukada, M.; Sugawara, T. *Mol. Cryst. Liq. Cryst*. **1993**, *232*, 103.

(7) Shiomi, D.; Nishizawa, M.; Sato, K.; Takui, T.; Itoh, K.; Sakurai, H.; Izuoka, A.; Sugawara, T. *J. Phys. Chem. B* **1997**, *101*, 3342.

(8) Numerical calculations for the spin Hamiltonian with larger number of spins are now in progress. Real-space spin−spin correlation function and temperature dependence of magnetic susceptibility calculated for the longer chains will be published elsewhere.

(9) Bencini, A.; Gatteschi, D. *EPR of Exchange Coupled Systems*; Springer-Verlag: Berlin, 1990; Chapter 3.

(10) Takahashi, M.; Turek, P.; Nakazawa, Y.; Tamura, M.; Nozawa, K.; Shiomi, D.; Ishikawa, M.; Kinoshita, M. *Phys. Rev. Lett.* **1991**, *67*, 746.

(11) For example, see: (a) Dietz, R. E.; Merritt, F. R.; Dingle, R.; Hone, D.; Silbernagel B. G.; Richards, P. M. *Phys. Rev. Lett.* **1971**, *26*, 1186. (b) Richards, P. M.; Salamon, M. B. *Phys. Rev. B* **1974**, *9*, 32. (c) McGregor, K. T.; Soos, Z. G. *J. Chem. Phys.* **1976**, *64*, 2506. (d) Turek, P. *Mol. Cryst. Liq. Cryst*. **1993**, *233* 191 and references therein.

(12) Slichter, C. P. *Principles of Magneitc Resonance*; Springer-Verlag: Berlin, 1990; Chapter 3.

(13) Shiomi, D.; Tamura, M.; Katori, H. A.; Goto, T.; Hayashi, A.; Ueda, Y.; Sawa, H.; Kato, R.; Kinoshita, M. *J. Mater. Chem.* **1994**, *4*, 915.